doi:10.1016/S0022-2836(03)00311-5 J. Mol. Biol. (2003) 328, 669–681

JMB

Available online at www.sciencedirect.com

SCIENCE DIRECT®

The X-ray Crystal Structure of Human β-Hexosaminidase B Provides New Insights into Sandhoff Disease

Timm Maier[1], Norbert Strater[1], Christina G. Schuette[2] Ralf Klingenstein[2], Konrad Sandhoff[2] and Wolfram Saenger[1]*

[1]*Institut für Chemie Kristallographie Freie Universität Berlin Takustr.6, 14195 Berlin Germany*

[2]*Kekule-Institut für Organische Chemie und Biochemie der Universität Bonn Gerhard-Domagk Str.1, 53121 Bonn, Germany*

**Corresponding author*

Human lysosomal β-hexosaminidases are dimeric enzymes composed of α and β-chains, encoded by the genes *HEXA* and *HEXB*. They occur in three isoforms, the homodimeric hexosaminidases B (ββ) and S (αα), and the heterodimeric hexosaminidase A (αβ), where dimerization is required for catalytic activity. Allelic variations in the *HEXA* and *HEXB* genes cause the fatal inborn errors of metabolism Tay–Sachs disease and Sandhoff disease, respectively. Here, we present the crystal structure of a complex of human β-hexosaminidase B with a transition state analogue inhibitor at 2.3 Å resolution (pdb 1o7a). On the basis of this structure and previous studies on related enzymes, a retaining double-displacement mechanism for glycosyl hydrolysis by β-hexosaminidase B is proposed. In the dimer structure, which is derived from an analysis of crystal packing, most of the mutations causing late-onset Sandhoff disease reside near the dimer interface and are proposed to interfere with correct dimer formation. The structure reported here is a valid template also for the dimeric structures of β-hexosaminidase A and S.

Keywords: hexosaminidase; Sandhoff disease; X-ray crystal structure; sphingolipid metabolism; *HEXB*

Introduction

The human β-hexosaminidases (EC 3.2.1.52) are lysosomal enzymes that degrade the carbohydrate moieties of glycoproteins, glycolipids and proteoglycans through the removal of terminal β-glycosidically linked *N*-acetylglucosamine or *N*-acetylgalactosamine residues. They are indispensable in human metabolism for the degradation of gangliosides, an essential class of outer-layer membrane lipids. The dimeric enzymes are composed of two subunits, α and β, that are approximately 60% identical in their amino acid sequence.[1,2] The subunits encoded by the genes *HEXA* and *HEXB* are synthesized as precursor proteins; processing and subunit assembly in the endoplasmatic reticulum yields three isoforms; β-hexosaminidase A (αβ, HexA), β-hexosaminidase B (ββ, HexB) and β-hexosaminidase S (αα, HexS). Dimerization of two chains is a prerequisite for the formation of catalytically active enzyme. Interestingly, the assembly of HexB from two β subunits is faster than the dimerization of α and β subunits to HexA. Thus, a pool of newly synthesized, unassembled α subunits is retained prelysosomally.[3,4] Properly folded and assembled enzymes are transferred rapidly to the Golgi apparatus for attachment of the mannose-6-phosphate recognition marker and targeted subsequently to the lysosomes, where final processing produces the mature enzymes.[5]

The wide substrate specificity of the A, B and S-isoforms of β-hexosaminidase is, at least in part, due to a unique active site carried by each subunit: the β-subunit predominantly hydrolyzes neutral substrates, whereas the α-subunit can cleave

Present addresses: N. Strater, Biotechnologisch-Biomedizinisches Zentrum der Universität Leipzig, Am Deutschen Platz 5, 04103 Leipzig, Germany; C. Schuette, Max-Planck-Institut für Biophysikalische Chemie, Abt. Neurobiologie, Am Fassberg 11, 37077 Göttingen, Germany.

Abbreviations used: Hex, β-hexosaminidase; hHex, human β-hexosaminidase; SpHex, *Streptomyces plicatus N*-acetylhexosaminidase; GM2AP, GM2 activator protein; SD, Sandhoff disease; δ-lactone, 2-acetamido-2-deoxy-D-glucono-1,5-lactone; SMChb, *Serratia marcescens* chitobiase; NAG, *N*-acetylglucosamine.

E-mail address of the corresponding author: saenger@chemie.fu-berlin.de

Table 1. Data collection, phasing and refinement statistics

Data collection	Pt	Hg	Native
Cell parameters (Å)	$a = b = 163.5$ $c = 244.7$	$a = b = 164.0$ $c = 245.1$	$a = b = 163.9$ $c = 244.7$
Wavelength (Å)	0.83432	0.83432	0.93400
Mosaicity (deg.)	0.298	1.061	0.466
Total reflections	465785	710539	1930354
Unique reflections	75615	77399	180325
Resolution (Å)	15–3.0	30–3.0	30–2.25
R_{sym} (%)[a,b]	12.6 (45.5)	14.2 (58.2)	6.5 (35.6)
Completeness (%)[a]	100 (100)	100 (99.9)	99.9 (100)
I/σ[a]	13.9 (4.0)	14.5 (3.3)	25.4 (5.5)
Number of sites	12	15	
R_{iso} (%)[c]	14.1	17.0	
Phasing power[d]	0.86/1.15	0.88/1.06	
Combined FOM[e]	0.54		
$\langle B_{Wilson} \rangle$ (Å^2)			32

Refinement	Native
R, R_{free}	0.196, 0.236
r.m.s.d. bonds (Å)	0.010
r.m.s.d. angles (deg.)	1.5
DPI[f] (Å)	0.30
Monomers/a.u.[g]	6
No. protein residues	2925
No. protein atoms	23,623
No. water molecules	2326
Heterogroups	6 δ-Lactone 18 *N*-Acetylglucosamine 18 Ethylene gycol
Solvent content (%)	53
$\langle B_{protein} \rangle$ (Å^2)	40 ± 11
$\langle B_{solvent} \rangle$ (Å^2)	50 ± 11

[a] Values for highest-resolution shells (Pt and Hg, 3.11–3.00 Å; native, 2.33–2.25 Å) are given in parentheses.
[b] $R_{sym} = \Sigma|I_{obs} - \langle I \rangle|/\Sigma\langle I \rangle$.
[c] $R_{iso} = \Sigma|F^2_{ph} - F^2_p|/\Sigma|F^2_{ph} + F^2_p|$.
[d] Phasing power (centric/acentric) = r.m.s. F_h/E_{iso}, where E_{iso} is the lack of closure error.
[e] FOM, figure of merit. $FOM = \langle cos(\Delta\alpha_h) \rangle$, where $\Delta\alpha_h$ is the error in the phase angle for reflection h.
[f] DPI, diffraction data precision indicator. DPI $= \sqrt{(N_{atoms}/N_{obs})(C - 1/3)d_{min}R_{free}}$, where N_{atoms} = number of atoms, N_{obs} = number of observations, C = fractional completeness and d_{min} = maximal resolution.
[g] a.u., Asymmetric unit.

negatively charged substrates.[6] The hydrolysis of ganglioside GM2 by HexA and of the sulfated glycosphingolipid SM2 by HexS requires coactivation by the GM2 activator protein (GM2AP). It lifts the gangliosides out of the membrane and presents their terminal sugar moieties to the water-soluble enzyme.[7,8]

The particular importance of human β-hexosaminidases is demonstrated by severe inborn errors of metabolism: mutations in the *HEXA* gene, which result in a lack of the isoforms HexA and HexS, cause Tay–Sachs disease; mutations in the *HEXB* gene lead to a deficiency of isoforms HexA and HexB and cause Sandhoff disease (SD). Both genetic disorders are characterized by a massive accumulation of ganglioside GM2 in neuronal lysosomes, leading to severe and, in most cases, fatal neurodegeneration.

The only structural information on human β-hexosaminidases available so far is a partial homology model based on the X-ray crystal structure of a related bacterial enzyme, *Serratia marcescens* chitobiase (SmChb), which belongs to family 20 of glycosyl hydrolases.[9] SmChb and other bacterial homologues differ significantly in structure and function from human β-hexosaminidases, being monomeric enzymes of a different substrate specificity as they degrade only water-soluble substrates. Also, the bacterial enzymes do not form ternary complexes with coactivator proteins and substrates, as observed for HexA and HexS. Thus, only limited insights into the unique and functionally decisive features of human β-hexosaminidases can be gained from analyzing the structures of bacterial homologues. To provide a structural basis for the understanding of folding, processing, dimerization and substrate specificity, we have determined the X-ray crystal structure of human β-hexosaminidase B (hHexB) at 2.3 Å resolution in complex with the transition state analogue inhibitor 2-acetamido-2-deoxy-D-glucono-1,5-lactone (δ-lactone).

Results and Discussion

Overall structural features

The crystal structure of hHexB, recombinantly expressed in insect cells, was determined by the

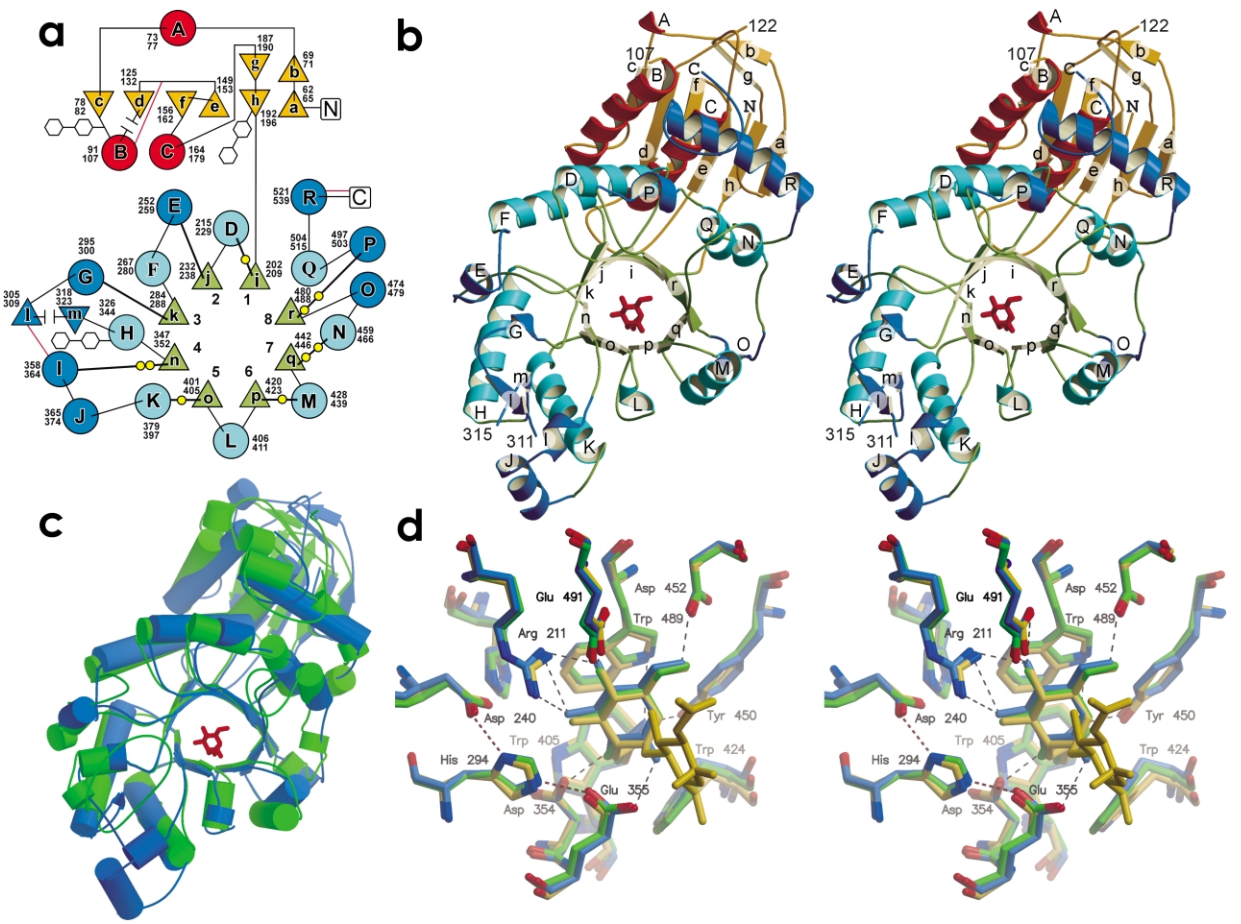

Figure 1. Fold and homologues of human β-hexosaminidase B. (a) Schematic topogram, α-helices are represented by circles, β-strands by triangles, numbers indicate the position in protein sequence. Glycosylation sites (hexagons), disulfide bonds (red lines), proteolytic cleavage sites of the mature human enzyme (┤├) and active-site residues (yellow circles) are indicated. (b) Ribbon diagram (stereo), N and C termini and proteolytic cleavage sites of processed HexB (107–122, 311–315) are indicated. In (a) and (b) the N-terminal domain is shown in orange (sheets) and red (helices), the C-terminal domain in green and cyan (strands and helices of central $(\beta,\alpha)_8$-barrel) and blue (extensions). In (b) the bound δ-lactone inhibitor is shown in red. (c) Least-squares superposition of hHexB (blue) with SpHex (green; pdb 1hp5) shown in cartoon representation. The view is identical with that in (b). (d) Least-squares superposition (stereo) of the active-site residues of hHexB (blue) in complex with δ-lactone, SpHex (green; pdb 1hp5) with the bound substrate chitobiose and SmChb (gold; pdb 1qbb) in complex with NAG-thiazoline. Residue labels relate to hHexB.

MIRAS method and refined to a crystallographic R/R_{free}-factor of 19.6%/23.6% at 2.3 Å resolution (Table 1). hHexB folds into two domains, an N-terminal α/β-domain and a central $(\beta,\alpha)_8$-barrel domain. α-Helices and β-strands are termed A to R and a to r, respectively; strands in the central $(\beta,\alpha)_8$-barrel are additionally numbered 1 to 8 in N to C-terminal order (Figure 1(a)). The N-terminal domain consists of a small two-stranded (b,g) and a larger six-stranded β-sheet (c,d,f,e,h,a) that is flanked by one short (A) and two long (B,C) α-helices, the latter forming the largest part of the interface to the central domain, while the opposite side of the large β-sheet is solvent-exposed (Figure 1(b)). The central domain is dominated by the $(\beta,\alpha)_8$-barrel that carries insertions (blue in Figure 1(a)) near strands 2 (j), 3 (k), 4 (n) and 8 (r) as well as a C-terminal helical extension (R). After strand 2 (j) as well as before and after strand 8 (r), single helices (E, O, P, respectively) are inserted, while the insertion after strand 3 (k) comprises one helix (G) and a two-stranded antiparallel β-sheet (l, m). Two adjacent helices (I, J) are inserted at the C terminus of strand 4 (n). All active-site residues are located in loops on the C-terminal side of the central $(\beta,\alpha)_8$-barrel (Figure 1(a) and (b)). According to the observed electron density and mass spectrometry, the enzyme is N-glycosylated at Asn84, Asn190 and Asn327 (indicated by linked hexagons in Figure 1(a)), but not at Asn142, while the enzyme purified from human placenta is glycosylated at all four sites.[10]

Structural homology to bacterial enzymes

The protein fold is highly conserved between hHexB and the bacterial members of family 20

glycosyl hydrolases with known structures; namely, a chitobiase from *Serratia marcescens* (SmChb)[9] and an *N*-acetylhexosaminidase from *Streptomyces plicatus* (SpHex).[11] Though sequence identity with SmChb and SpHex is only 22% and 27%, respectively, the positions of secondary structure elements of the C-terminal $(\beta,\alpha)_8$-barrel and, unexpectedly, the N-terminal domain are well conserved in hHexB (Figure 1(c)). While SmChb contains two extra domains, extending the protein N and C-terminally, SpHex contains only the domains shared with hHexB. Structural alignments of SmChb/SpHex with hHexB identify 344/349 (71%/72% of residues in hHexB) matching residues with an r.m.s.d. between the C^{α} atoms of 1.4 Å/1.5 Å. However, both bacterial enzymes are monomeric and have different substrate specificities compared to the dimeric human β-hexosaminidases. Though all catalytically essential residues are conserved, most of the loops on the C-terminal face of the $(\beta,\alpha)_8$-barrel are in different conformations or of different length in the bacterial enzymes (Figure 1(c) and (d)). Consequently, these loops are modelled incorrectly in the homology model of hHexB, which includes the C-terminal $(\beta,\alpha)_8$-barrel, but not the N-terminal domain and the C-terminal residues beyond helix Q. Thus, the r.m.s.d. for an all-atom or C^{α} atom superposition of the homology model (pdb 1qbd) onto the hHexB crystal structure is high, 3.6 Å or 3.0 Å, respectively.

Catalytic mechanism: the transition state

The crystal structure of hHex B is in agreement with the suggested conservation of a common

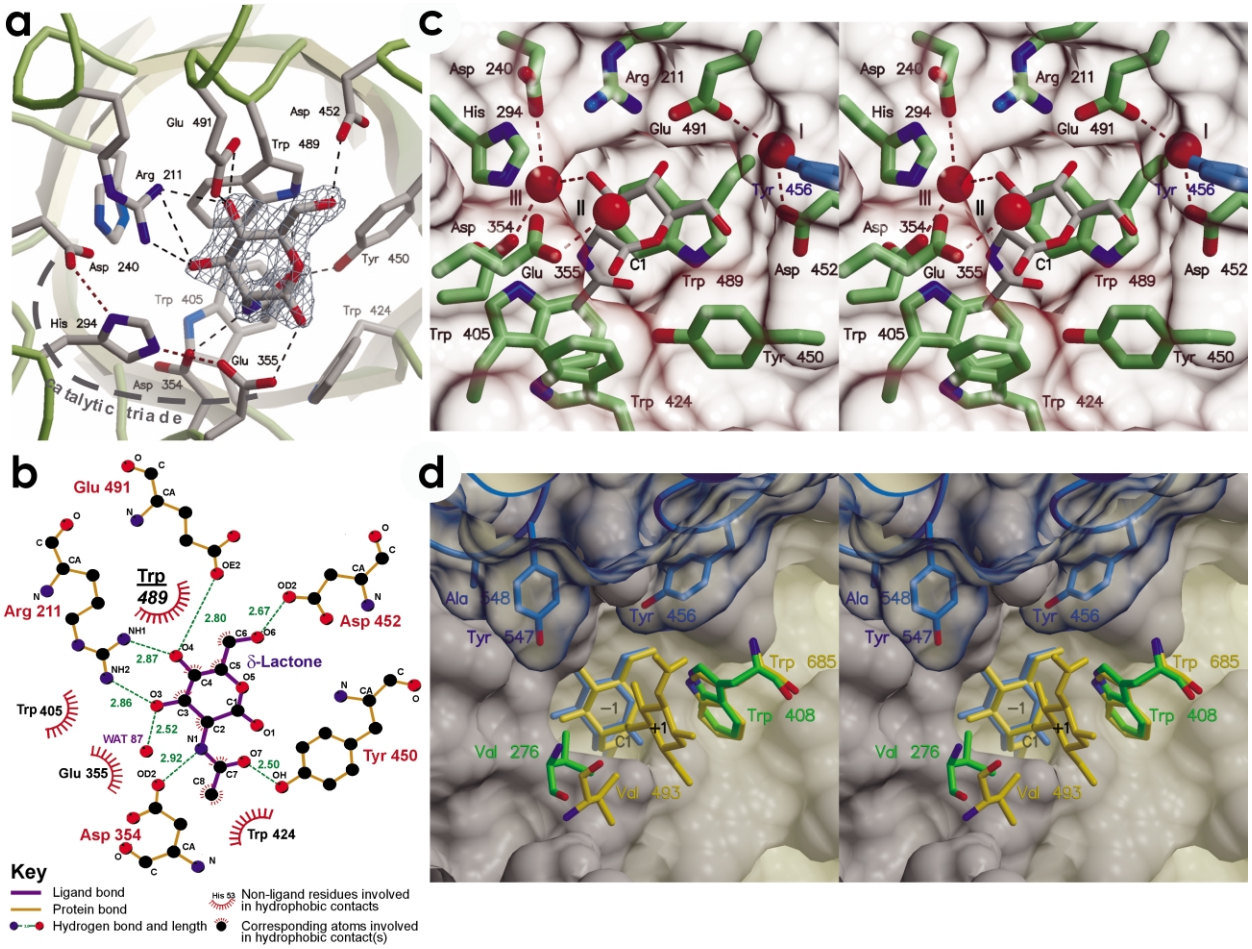

Figure 2. Active site and inhibitor interactions. (a) The active site is shown in ribbon-and-stick representation. The electron density ($F_o - F_c$ omit map around the inhibitor) is contoured at the 1.5σ level. The view in (a) and (b) is identical with that in Figure 1(d). (b) Interactions between active-site residues and the bound δ-lactone inhibitor. The hydrophobic stacking partner of the bound inhibitor, Trp489, is highlighted. (c) Stereo view of the bound inhibitor shown in stick representation together with three surrounding water molecules, I-III, represented by spheres. Covered by a semitransparent solvent-accessible surface, protein residues important for substrate binding are shown. Tyr456 (blue) belongs to the other subunit of the dimer. Only selected hydrogen bonds involving the three water molecules are indicated. (d) The solvent-accessible surface of one monomer of hHexB is shown in solid grey, the surface of the second subunit is shown in transparent blue. The δ-lactone inhibitor, which is bound to the first dimer subunit and close residues from the second subunit are shown in blue. Residues coordinating the +1 sugar of chitobiose, co-crystallized with SmChb, in SmChB (gold; pdb 1qbb) and corresponding residues in SpHex (green; pdb 1hp5) are superimposed on the hHexB structure based on the fit shown in Figure 1(d).

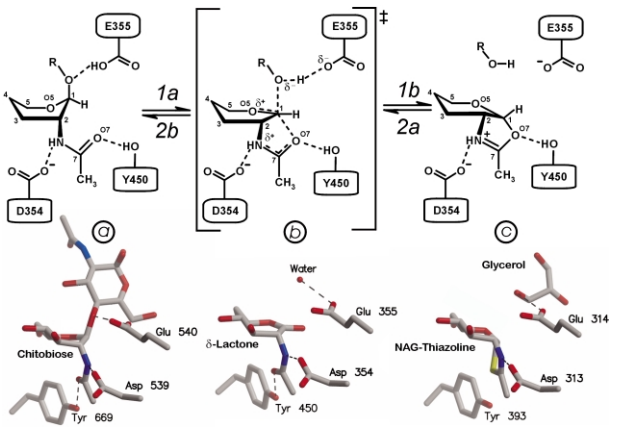

Figure 3. Catalytic mechanism of human β-hexosaminidase B. The sketch in the upper panel illustrates the two-step double-displacement mechanism: in the first step (*1a*, *1b*) (R = carbohydrate) a substrate-mediated nucleophilic attack on C1 is assisted by the general acid–base catalyst Glu355 and releases the residual carbohydrate R *via* the formation of a cyclic oxazolinium intermediate. In the second step (*2a*, *2b*) (R = H) a water molecule activated by Glu355 carries out a nucleophilic attack on C1 to open the oxazolinium ring, thereby retaining the initial configuration at C1. In the lower panel, all steps of the mechanism are illustrated by X-ray crystal structures: (a) SmChb together with the substrate chitobiose (pdb 1qbb); (b) hHexB in complex with δ-lactone inhibitor (this work); (c) SpHex in complex with NAG-thiazoline; here, the water position is occupied by a glycerol molecule (pdb 1hp5).

catalytic mechanism with the bacterial hexosaminidases. The family 20 glycosyl hydrolases share a configuration retaining double-displacement mechanism with a substrate-mediated nucleophilic attack. It is the acetamido oxygen atom of the terminal non-reducing −1 sugar of the substrate itself that carries out the nucleophilic attack on the anomeric C1, as has been demonstrated by the crystal structures of SpHex in complex with chitobiose (di-*N*-acetylglucosamine, di-NAG) and of SmChb in complex with the potent inhibitor NAG-thiazoline.[9,11,12] The −1 subsite, binding the non-reducing sugar, of the substrate pocket is almost identical between these enzymes and hHexB (Figures 1(d) and 2(a) and (b)). The proposed double-displacement mechanism involves two steps (Figure 3):

In the first step (Figure 3, reaction *1a*, *1b*, R = carbohydrate), the acetamido oxygen atom of the non-reducing −1 sugar molecule is forced into an optimal position by Asp354, Tyr450 and Trp424 (Figures 2(c) and 3, state (*a*)) and attacks as a nucleophile the anomeric C1 of the same sugar molecule to form an oxazolinium intermediate and to release the deprotonated +1 sugar molecule; Glu355 protonates the departing carbohydrate. While the terminal non-reducing sugar molecule binds to the −1 site in a distorted boat conformation (Figure 3, state (*a*)), it relaxes to a $^4C_1$ chair conformation in the oxazoline intermediate (Figure 3, state (*c*)). In a second step (Figure 3, reaction *2a*, *2b*, R = H) the general acid–base catalyst Glu355 activates an incoming water molecule,[13] which attacks the anomeric C1 of the −1 sugar molecule and hydrolyzes the oxazolinium ion ring while retaining the initial configuration of the sugar. Glu355 is part of a hydrogen bonded catalytic triad, formed together with His294 and Asp240 (Figure 2(a)). The reported complex of SmChb with di-NAG represents a substrate-like structure, whereas the NAG-thiazoline bound to SpHex is a hydrolytically stable analogue of the oxazolinium intermediate. In contrast, in the hHexB complex, the potent inhibitor δ-lactone with its planar carboxyl group resembles the transition state of the non-reducing −1 sugar molecule in the moment the anomeric C1 traverses the plane defined by C2, C5 and O5 of the sugar ring (Figure 3, state (*b*)). The structure reported here demonstrates that the transition of C1 does not require or induce any change in the geometry of the substrate-binding pocket.

Two possible candidates for the incoming water molecule attacking C1 in the oxazolinium ring in the second step of the double-displacement mechanism were suggested from the crystal structures of SmChb and SpHex and are found in the hHexB·δ-lactone complex (Figure 2(c)): a first water molecule, I, in the SmChb structure hydrogen bonded by Glu739 (Glu491 in hHexB) and Asp671 (Asp452 in hHexB)[9] and a second, hypothetical, water molecule, II, in a bulk solvent-exposed position in a site occupied by a glycerol oxygen atom hydrogen bonded to Glu314 (Glu355 in hHexB) in the structure of SpHex.[11] Both potential water sites are occupied by water molecules in all six monomers in the asymmetric unit of hHexB crystals.

Water molecule I (Figure 2(c), I) has an average *B* value of 33.0 Å^2 and is fixed in its position by short hydrogen bonds to $O^{\delta 2}$ of Asp452 and $O^{\epsilon 1}$ of Glu491. Remarkably, this water molecule is coordinated also by the hydroxyl O^{η} of Tyr456 of the other subunit of the dimer (see below) at a distance of 2.7 Å. The coordination sphere would allow interpretation of this water position as a sodium ion. The strong coordination suggests a structural role for this water molecule, similar to that of a second conserved water molecule coordinated by Asp240 and Asp354, which is involved directly in ligand binding by forming a hydrogen bond to O3′ of the δ-lactone inhibitor (Figure 2(c), III). Both of these water molecules are buried once a substrate molecule is bound. Water molecule II (Figure 2(c), II) is coordinated and activated by Glu355 and has a higher average *B* value of 55.3 Å^2, corresponding to greater mobility or partial occupancy. It is well positioned for an inline attack on the anomeric C1 in the oxazolinium intermediate with an interatomic distance of 3.2 Å to the C1 atom of the transition-state analogue inhibitor δ-lactone. Even with the non-reducing

sugar molecule bound to the −1 subsite, this water molecule is solvent-exposed and water molecules from the bulk solvent could easily enter this position after departure of the residual carbohydrate chain (Figure 2(c)). Therefore, we identify water molecule II as the nucleophilic water molecule attacking the intermediate oxazolinium ring to form the final product in the second step of catalysis (Figure 3).

Crystal packing and quaternary structure

Until now, the dimer structure of human hexosaminidases and its influence on substrate specificity has remained an open question. To identify the physiologically active dimer (for a review, see Gravel *et al.*[5]), it is necessary to distinguish between intermolecular crystal packing contacts and the interface of the dimer, which is observed in solution. The crystal packing of hHexB is complex, with the crystal asymmetric unit containing six monomers, organized in three pairs of molecules related by non-crystallographic 2-fold rotation axes. Aside from a few weak contacts involving no more than five residues in each interacting monomer, three intermolecular interfaces are observed, numbered I to III in decreasing interaction strength (Table 2). Interface I involves a larger number of contacting residues (24) than either II (13) or III (11), and an approximately two-fold greater buried surface area per monomer (1368 Å^2) and number of involved hydrophobic residues (eight residues). Although interface I is formed mainly by loop regions, the average *B* value of its residues is significantly lower (B_{aver} = 33 Å^2) than for interfaces II (B_{aver} = 40 Å^2) and III (B_{aver} = 49 Å^2); lower, even, than the average *B* value for all protein residues (B_{aver} = 40 Å^2) (Table 2; Figure 4(a) and (b)). Both the buried surface area and the number of hydrogen bonds between the monomers in interface I are close to the typical values obtained in a survey of 36 permanent protein complexes.[14] More amino acid residues involved in formation of interface I are identical (63%) between different mammalian α and β-subunits than those comprising interfaces II and III (23% and 18%, Table 2). Therefore, only interface I favors the formation of equivalent dimers in HexS (αα), HexA (αβ) and HexB (ββ). Out of all possible monomer–monomer interfaces, only I positions side-chains of one subunit (e.g. Tyr456, colored blue in Figure 2(c)) in the vicinity of the active site of the other subunit, thus making the regulation of substrate specificity by an interaction partner plausible, as is demonstrated by the different activities of the α-subunits in HexS and HexA against SM2.[8] Thus, the physical strength of the interaction and biological evidence qualifies interface I as a physiologically valid dimer interface, while the others must be regarded as crystal packing interactions.

Table 2. Properties of intermolecular interfaces I–III observed in hHexB crystals

Properties	I (AB)	II (AC)	III (BC)
Residues involved in each monomer	211,212, 260	78	71–75
	452–456	89,92,96,99	123
	491,492,494 496,497	247,249	183,184
	500,501, 533	262,265,267	186,187
	543–550	269,270,273	552
No. of residues[a,b]	24	13	11
Non-bonded contacts	59	8	7
No. hydrophobic residues[a,c]	8	3	3
Hydrogen bonds	10	10	3
per 100 Å^2 area	0.73	1.33	0.63
Residues identical (%)[d]	63	23	18
Residues conserved (%)[d]	25	38	36
Average *B* value (Å^2)	33 ± 4	40 ± 6	49 ± 10
Buried surface (Å^2)[a]	1368	751	473

[a] Values are given per interface side.
[b] Interface residues contain atoms closer than 3.66 Å to atoms of the interface partner.
[c] Hydrophobic residues are Ile, Leu, Val, Met, Tyr, Phe and Trp.
[d] Conservation between all human and murine hexosaminidase α and β-chains.

The dimer interface

The proposed dimer interface is formed mainly by loop regions at the C-terminal face of the $(\beta,\alpha)_8$-barrel, as is the active site. The contributing loops are located between strand i and helix D, helices E and F, strand q and helix N, and strand r and helix P. Furthermore, helix P and the C-terminal loop residues from 543 to 550 contribute to the dimer interface. The interface itself is approximately rectangular, with dimensions of 45 Å^2 × 25 Å^2. The most striking feature of the interface is a crescent formed by five tyrosine residues (Figure 4(c)). Each of these forms, among other interactions, hydrophobic contacts to one of the five tyrosine residues in the interface region of the other subunit. Contacts of other non-polar side-chains, e.g. those of Leu453, Pro545 and Leu546 (colored dark grey in Figure 4(c)), with one of the five tyrosine residues comprise further hydrophobic interactions. Hydrogen bonding contributes to the dimer interactions to a lesser extent, being observed in only four side-chain–side-chain and one main-chain–side-chain, but no main-chain–main-chain interaction (Figure 4(d)). A considerable number of ordered water molecules is embedded between the two subunits forming hydrogen bonds to residues of both chains.

Anatomy of the substrate-binding site

Though the active center and the binding site of the non-reducing sugar molecule −1 are highly conserved between hHexB and the bacterial homologues, the remainder of the substrate-binding site is significantly different. In the bacterial

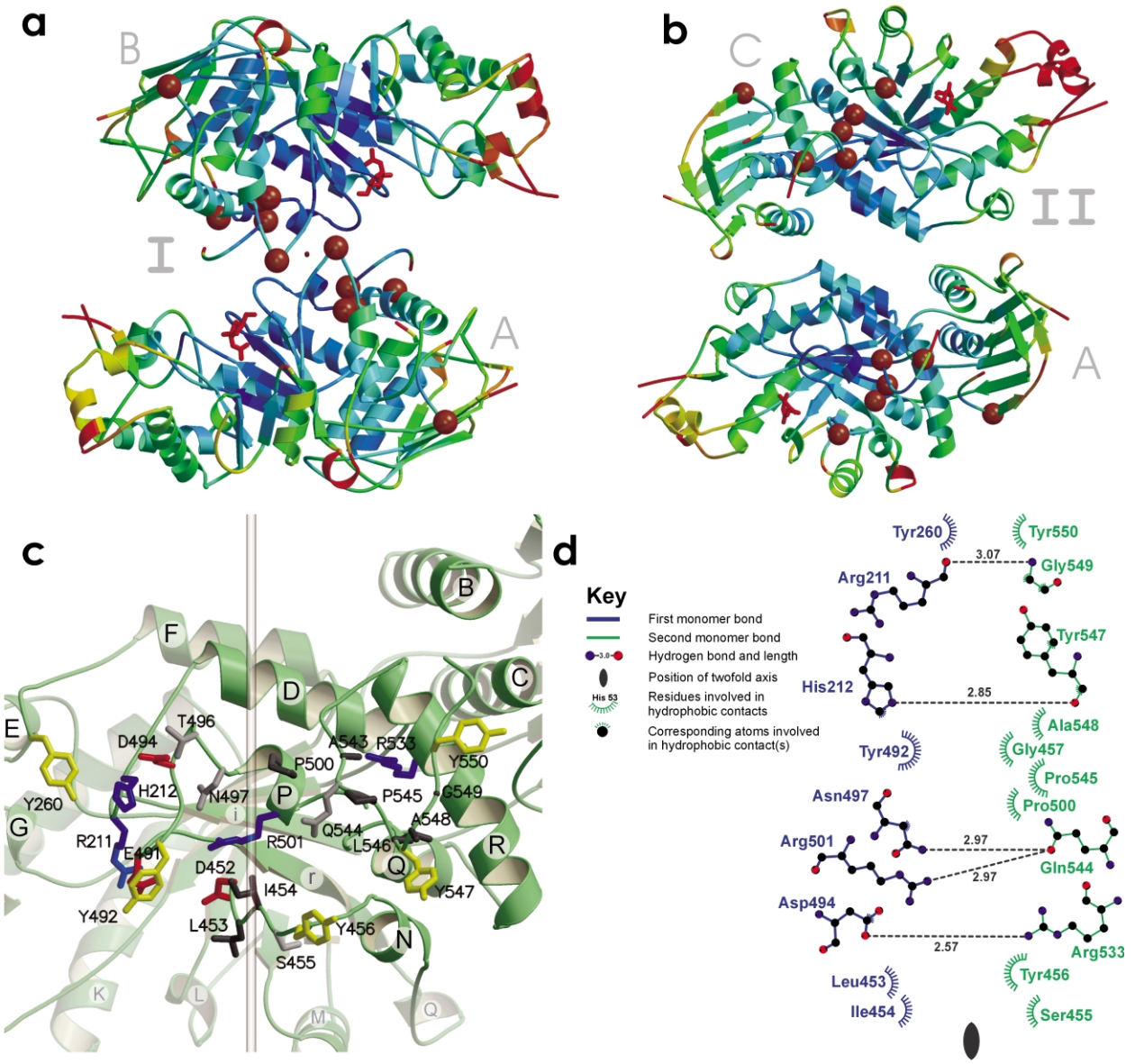

Figure 4. Crystal packing and dimerization. (a) Interface I (molecules A and B), viewed along the 2-fold rotational dimer axis. (b) Interface II (molecules A and C), the view is perpendicular to that in (a). In (a) and (b), ribbon representations are colored according to increasing temperature factors, from blue to red. The bound inhibitor molecules are shown in red. Positions of disease-associated mutations are indicated by red spheres around the corresponding C^{α} atoms. (c) The dimer interface (as shown in (a)) of molecule A (green). Interface residues are shown as sticks, non-polar residues are colored dark grey, polar non-ionic residues light grey, cationic residues blue and anionic residues red. Tyrosine residues forming a crescent around the interface are shown in yellow. The 2-fold rotation symmetry axis is shown as a transparent stick. (d) A representation of the dimer interface; only major interacting residues are shown. They represent half of the dimer contacts; the second half is generated by a 2-fold rotation symmetry axis, which is perpendicular to the paper plane, indicated by a black ellipse.

enzymes, the +1 sugar molecule is bound to a conserved tryptophan residue, Trp685 and Trp408 in the Sm and Sp enzymes, respectively, *via* hydrophobic stacking interactions. The walls of the sugar-binding crevice are formed by hydrophobic residues in similar positions in SmChB and SpHex; namely, Val493/Val276 (Sm/Sp) on the opposite side and Tyr683/Leu406 on the same side of the +1 sugar ring as compared to the conserved tryptophan residue. No equivalent of these residues binding the +1 sugar ring is present in hHexB (Figure 2(d)). The binding pocket of the human enzyme encloses only the −1 sugar molecule tightly and is wide open around the +1 sugar molecule and following groups in the natural substrates such as glycolipid GA2. A different binding mode for the natural substrates of human hexosaminidases compared with the chitobiose binding of bacterial enzymes is unlikely, as it would interfere with the conserved double-displacement mechanism. Only the binding of the substrate in a distorted sofa conformation, instead

of a relaxed $^4C_1$ chair one, brings the glycosidic atom O1 in close proximity to the general acid–base catalyst Glu355 (Figure 3). It still remains unclear whether parts of the larger natural substrates beyond the first sugar residue −1 interact with hHexB. In the case of HexA and HexS, it is assumed that most atoms of the substrates, sugar as well as lipid moieties, are in contact with GM2AP[15] and only the terminal sugar molecules are bound by hexosaminidases.

Allelic variations of the *HEXB* gene

Genetic defects causing SD include partial gene deletions, smaller insertions and deletions, and individual base substitutions in the *HEXB* gene. Mutations leading to no or highly unstable mRNA are associated with early onset of disease symptoms and a fatal clinical course. Point mutations allowing the production of mRNA and protein with residual activity cause less severe cases of SD, with late onset and slow progression of the disease. Several of these point mutations in hHexB were detected in patients suffering from SD (Table 3).[5]

All residues whose mutations impair protein function are very well ordered in the crystal structure of hHexB, with *B* values lower than the average for all residues (Figure 4(a)). The functional importance of these residues has been discussed,[9] but with only limited information as the homology model used lacked the N-terminal domain and the C-terminal residues involved in the dimer interface. Moreover, most loops of the dimer interface were modelled incorrectly and protein-protein interactions in the dimer were not known or considered, although human β-hexosaminidases are active only in the dimeric form. Because most observed mutations are located in regions of dimer contacts or disturb the dimer interface structure indirectly (Figure 4(a)), as will be discussed for the individual mutations in the following paragraphs, the previous model based analysis has proven insufficient.

Of those residues associated with pathogenic mutations, only Pro504 and Arg505 are highly conserved in related eukaryotic and prokaryotic enzymes, while Pro417, Tyr456, Cys309, Cys534 and Ala543 are conserved only in mammalian α and β-chains. As the active site and the catalytic mechanism of eukaryotic and prokaryotic homologues are virtually identical, this again points to the importance of dimerization properties as a key to understanding the function of hHexB.

Mutation Ser62Leu: infantile acute SD

The nucleotide exchange C185T resulting in a Ser62Leu mutation in the hexosaminidase β-chain was found in one allele of an infantile onset SD patient with a partial deletion of the *HEXB* gene in the second allele.[16] No report exists on the expression or activity of the mutant enzyme. Ser62 is located in a sharp β-turn at the N terminus of the N-terminal β-strand a. While serine is one of the residues that strongly favors a turn conformation, leucine disfavors it, as reflected by their Chou–Fasman turn parameters of 143 for Ser and 59 for Leu.[17] This suggests an influence of the amino acid substitution Ser62Leu on the overall folding of HexB, as the turn is essential to keep the fold of the N-terminal domain intact.

Mutation Pro417Leu: subacute or chronic SD due to missplicing

The nucleotide exchange C1214T in exon 11 of the *HEXB* gene leads to the production of an unstable and misspliced mRNA and thus to lowered expression levels of HexB. However, the mutant protein expressed in COS cells also shows only 70% of the specific activity of the wild-type enzyme.[18] This mutation is similar in nature to Ser62Leu, as a proline residue in a β-turn is replaced by a leucine residue that disfavors loop conformations. The Pro417Leu mutation has been observed in patients together with a Cys309Tyr mutation, which blocks the formation of a disulfide bond,[19] and a common polymorphism Lys121Arg.[20] The combination of these mutations potentially has a stronger effect on the activity of hHexB than a single Pro417Leu mutation.

Table 3. Point mutations in the hexosaminidase β-chain detected in Sandhoff disease patients

Mutation	Biochemical phenotype	Clinical phenotype	Reference
S62L	Unknown	Infantile acute (second allele del50kb)	16
C309Y	Unknown	Chronic (probably due to second allele P417L)	19
P417L	70% of normal activity in mutant expressed HexB	Subacute or mild chronic	19,20,43
Y456S	HexB absent, β chains only in HexA, HexA activity: 30% of wild type	Subacute (second allele I207V)	21,44
P504S	Approx. 20% activity against MUG, mainly in proenzyme form	Chronic (second allele del16kb)	23
R505Q	Thermolabile	Chronic (second allele null)	22
C534Y	Unknown	Infantile acute	24
A543T	Thermolabile	Asymptomatic	26
K121R	Unaffected	Polymorphism	20
I207V	Unaffected	Polymorphism	16

Mutation Tyr456Ser: subacute or chronic SD

Two mutations in the hexosaminidase β-chain were observed in a patient suffering from a juvenile onset motor neuron disease, a paternally inherited Ile207Val and a maternally inherited Tyr456Ser mutation.[21] The Ile207Val mutation has been characterized as a common polymorphism not associated with diminished enzyme activity or SD.[16] Tyr456 is located in a loop on the C-terminal side of strand q (strand 7 of the $(\beta,\alpha)_8$-barrel; Figure 1(a)), close to the active-site residues Tyr450, Asp452 and Leu451, the latter being affected also by the Arg505Gln mutation (see below). Thus, one possible effect of the mutation is a change in loop conformation affecting the active-site geometry, though the distance between Tyr456 and the bound ligand is about 20 Å (Figure 5(a)). As mentioned above, Tyr456 plays an important role in dimerization, where it forms strong hydrophobic interactions with Ile454 and Tyr492 of the other subunit, and is located on the crescent around the dimer interface (Figure 4(c)). These contacts aid in the fixation and positioning of loops on the C-terminal sides of strands q and r (strands 7 and 8 of the $(\beta,\alpha)_8$-barrel) carrying active-site residues of the other subunit. The importance of Tyr456 for dimerization is confirmed by biochemical data: the absence of active HexB from cultured fibroblasts of an SD patient carrying the Tyr456Ser mutation together with the presence of β-chains in active HexA suggests a defect in homodimerization of the mutant β-chains.[21] Moreover, Tyr456 protrudes as a tyrosine finger towards the substrate bound in the second subunit, such that its hydroxyl group is at a distance of just 4 Å from the closest atom of the inhibitor δ-lactone (Figures 2(d) and 5(a)). The Tyr456 hydroxyl O^{η} coordinates a structural water molecule, which is coordinated also by Asp452 and Glu491 of the other monomer, as discussed above (Figures 2(c) and 5(a)). Therefore, Tyr456 may indirectly influence the active-site structure of the other subunit and is a potential binding partner for larger and natural substrates. A mutation to the smaller serine would abolish the hydrophobic intermolecular contacts formed by the bulky aromatic tyrosine ring and may affect the stability of the HexB dimer, as well as the geometry of the catalytic site on both subunits of the dimer.

Mutations Pro504Ser and Arg505Gln: heat-labile HexB and chronic SD

Bolhuis *et al.*[22] identified the mutation Arg505Gln in the β-chain of HexB as the molecular basis for an adult onset form of SD. This variant enzyme was expressed in COS cells and its activity was found to be heat-labile as compared to the wild-type enzyme. Arg505 is located at the N terminus of helix Q and short hydrogen bonds are formed between its guanidyl nitrogen atoms $N^{\eta}H1$ and $N^{\eta}H2$, and the backbone oxygen atom of Leu451. Residue Leu451 is located in a loop at the C terminus of strand q (strand 7 of the $(\beta,\alpha)_8$-barrel) and its direct neighbors Tyr450 and Asp452 play important roles in substrate binding (Figure 2(a) and (b)). We suggest that the hydrogen bond between Arg505 and Leu451 is essential to stabilize the strongly bent loop conformation around Leu451 and thus to maintain the geometry of the −1 sugar-binding site. The guanidyl $N^{\eta}H1$ of Arg505 forms a short hydrogen bond to the backbone oxygen atom of Arg501 located in helix P. Arg501 itself is involved directly in dimerization: a hydrogen bond is formed between its guanidyl $N^{\eta}H2$ and the side-chain $O^{\epsilon 1}$ of Gln544 in the other subunit (Figures 4(d) and 5(b)). Therefore, Arg505 acts together with Tyr456 as a second direct link between dimerization and active-site structure. A mutation of the neighbouring residue of Arg505, Pro504, to serine results in the expression of heat-labile HexA with reduced activity towards

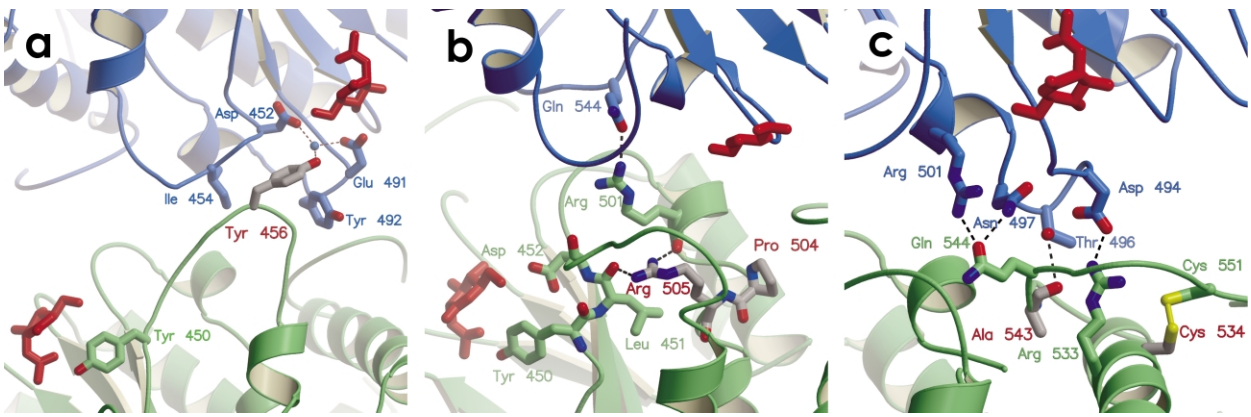

Figure 5. Overview of residues associated with pathogenic mutations. The hHexB subunit carrying the mutation associated residue(s) is shown in green, the other one in blue. Residues mutated in pathogenic variants are colored grey and labelled red. The cocrystallized δ-lactone inhibitor is shown in red. Only selected residues are shown. (a) Tyr456; (b) Pro504 and Arg505; (c) Cys534 and Ala543.

its natural substrates, but not towards small artificial substrates.[23] This indicates that the mutation affects substrate binding, but not catalytic turnover. Pro504 is located at the beginning of a β-turn and adopts a *cis*-peptide conformation. A serine residue is unlikely to accommodate a similar conformation and will consequently distort the loop conformation. Such alterations would change the orientation of the neighboring C-terminal loop that forms major parts of the dimer interface, as well as the positioning of the adjacent residue, Arg505, discussed above (Figure 5(b)).

Mutation Cys534Tyr: infantile acute SD

Kuroki *et al.*[24] have found a patient with infantile SD to be homozygous for a *HEXB* mutation resulting in a Cys534Tyr substitution, originally described as Cys522Tyr. Cys534 of the hexosaminidase β-chain forms a disulfide bond to Cys551,[10] which fixes the C-terminal loop to the C-terminal core domain of the protein. Considering one monomer only, the non-disulfide bonded C-terminal loop is expected to be disordered and solvent-exposed as residues 547–552 have no contact to the rest of the protein except the disulfide bond involving Cys551. In the active dimer, these C-terminal residues form an integral part of the dimer interface and all residues from 543 to 550, i.e. to the disulfide bonded Cys551, form interchain contacts. The mutation of Cys534 to tyrosine leaves the C terminus conformationally unrestrained and affects a large portion of the interaction potential between the two subunits of the dimer (Figure 5(c)).

Mutation Ala543Thr: heat-labile HexB

Upon incubation at 50 °C for three hours, HexA is inactivated completely, whereas HexB activity remains unchanged. This heat-stability of HexB is commonly used to differentiate it from HexA. However, a heat-labile form of HexB was identified by Navon & Adam,[25] which occurs in different frequencies among various population groups and exists in unaffected persons as well as some SD patients. Narkis *et al.*[26] identified the underlying mutation G1627A in the *HEXB* gene as causing an Ala543Thr change in HexB. Residue Ala543 is part of the dimer interface and a hydrogen bond is formed between its backbone oxygen atom and O^{γ} of Thr496 of the other subunit. Additionally, the neighboring residues in sequence and space, Arg533 and Gln544, both form hydrogen bonds to side-chains of residues of the other dimer subunit, Asp494 for Arg533 and Asn497, Arg501 for Gln544. The change of Ala543 to the bulkier Thr543 is expected to affect the packing of this residue and consequently distort the geometry of the dimer interface, explaining the heat-lability of the resulting HexB variant (Figure 5(c)).

Conclusion

We report here the crystal structure of recombinantly expressed, homodimeric human β-hexosaminidase B with a glycosylation pattern nearly identical with that of the enzyme purified from human placenta.[10] On the basis of this crystal structure, the function of individual amino acid residues mutated in patients suffering from Sandhoff disease has been discussed. Most of these residues are involved in formation of the proposed dimer interface directly (Tyr456, Ala543) or indirectly (Pro504, Arg505, Cys534). Residues Tyr456 and Arg505 even act as direct links between the geometry of the active site and the structure of the dimer interface. Remarkably, 20 out of 25 residues in the dimer interface are identical between the β and α-subunits of human β-hexosaminidases and two more residues are conserved, though most of these residues are located in loop regions (data not shown; details of the alignment are available from the authors upon request). The insights concerning dimerization properties are thus not limited to HexB but will also provide a key to the mechanism by which the substrate specificities of HexA and HexS are determined.

The availability of structural details of the complete binding site beyond the −1 sugar-binding site facilitates understanding of the interaction of HexB with larger natural substrates. GM2AP binds to HexA and HexS, and stimulates substrate hydrolysis but does not act on HexB.[5,7,8,27] Based on the crystal structure presented here, residues in the vicinity of the active site on both monomers of the dimer can be identified, which are not conserved between the α and β-chains of β-hexosaminidases. These will be the primary targets of mutational studies to analyze the binding of GM2AP protein to hexosaminidases. Together with the known X-ray crystal structure of GM2AP,[15] models for the ternary complex of natural substrate, GM2AP and β-hexosaminidase can be constructed by computer modelling that will guide future biochemical investigations on the mode of coactivation in glycolipid degradation by β-hexosaminidases. Furthermore, the structure of hHexB will aid in the rational design of hexosaminidase inhibitors recently described as promising drug candidates for the treatment of osteoarthritis.[28] To render such inhibitors nontoxic, they must be as specific as possible. HexS acts on glycosaminoglycans,[8] which are of particular interest in osteoarthritis development. The −1 sugar-binding site of the α-subunits in HexS and HexA are identical, but the different dimerization partners in both enzymes will lead to structural differences in the surrounding of the active sites. These differences can be exploited in the rational design of isoform-specific inhibitors of hexosaminidases. The future potential of structure determination of recombinant hHexB is therefore not limited to an extended molecular understanding of the hexosaminidase related genetic diseases.

Materials and Methods

Crystallization and X-ray data collection

Human β-hexosaminidase B (hHexB) was expressed using a recombinant baculovirus expression system and purified as described.[10] The hanging-drop, vapor-diffusion method was used for crystallization. The reservoir solution was 100 mM sodium citrate buffer (pH 5.6), 16% (v/v) ethylene glycol, 10% (v/v) polyethylene glycol 8000. The protein solution contained 10 mg/ml of hHexB in 10 mM sodium citrate (pH 6.0), 100 mM NaCl. The drop was formed by adding 4 μl of protein solution and 1 μl of 5 mM 2-acetamido-2-deoxy-D-glucono-1,5-lactone (δ-lactone; Toronto Research Chemicals Inc., Toronto, Canada) to 5 μl of reservoir solution. Crystals of a size of 0.1 mm × 0.1 mm × 0.4 mm were transferred to a cryobuffer (100 mM sodium citrate buffer (pH 5.6), 30% ethylene glycol, 12.5% polyethylene glycol 8000, 0.5 mM δ-lactone) and flash-cooled in liquid nitrogen. For heavy-atom derivatization, crystals were soaked overnight in cryobuffer containing 1 mM K_2PtCl_4 (Pt) or 1 mM $HgCl_2$ (Hg) prior to flash cooling. Crystals belong to space group $P3_121$ with cell parameters $a = b = 164$ Å and $c = 245$ Å. Crystallographic data were collected at 100 K at BAMline, BESSY (Berlin, Germany) and at ID14EH1, ESRF (Grenoble, France). Details of data collection and reduction are given in Table 1.

Structure solution, refinement and analysis

HKL Suite[29] was used for data reduction. Initial phases were obtained with SOLVE[30] in a MIRAS protocol using the Pt and Hg datasets in the resolution range 20–4 Å (Table 1). Phases were improved by electron density modification and NCS-averaging with DM[31] exploiting the observed 6-fold non-crystallographic symmetry. Phase extension to 2.25 Å resolution with a native dataset yielded well-interpretable experimental maps of extraordinary quality. The model was built with O,[32] refinement was carried out with CNS[33] using simulated annealing and conjugate gradient minimization against maximum likelihood targets including bulk solvent correction. Individual B values were refined for all non-hydrogen atoms. The final model included six protein chains, each composed of three fragments of residues 54–107, 122–311 and 315–552/553. The C-terminal residues up to 556 and residues 42–53 on the N terminus are disordered, the N terminus of the mature human enzyme is located at residues 48–50. Due to the expression in insect cells, HexB is not processed proteolytically by removal of residues 108–121 and 312–314 as the mature human enzyme. However, the loop 108–121 is excised partially during purification, as demonstrated by SDS-PAGE (data not shown) and no electron density was found for either loop; thus, they are disordered in the crystal. The protein is N-glycosylated at residues N84, N190 and N327. No glycosylation is observed at N142, in contrast to the enzyme purified from human placenta.[10] Three intrachain disulfide-bridges are formed between residues Cys91 and Cys137, Cys309 and Cys360, and Cys534 and Cys551. Alternate conformations were observed for 28 residues, amongst them several cysteine residues in the free instead of the expected[10] disulfide bonded form. The opening of these disulfide bonds is attributed to radiation damage during the X-ray experiment.[34] The C-terminal three or four amino acid residues are disordered and not visible in the electron density maps. One molecule of the inhibitor δ-lactone is bound to each protein chain. The R/R_{free} values for the final refined model including 2925 amino acid residues, 42 non-protein residues (six δ-lactone, 12 ethylene glycol, 24 *N*-acetyl-glucosamine) and 2326 water molecules are 0.196/0.236. In the Ramachandran plot, 89.6% of all amino acid residues are in the most favored, 10.1% in additionally allowed, 0.2% in generously allowed and 0.0% in disallowed regions. The refined average atomic B factor for all protein residues of 40 Å^2 is slightly higher than the Wilson plot B factor of 32 Å^2 (Table 1). This difference may be explained by anisotropic disorder, the applied scaling protocols or the larger number of less well ordered chain termini due to the presence of multiple chains in the asymmetric unit.

Structural alignments were carried out with CE.[35] Hydrogen bonding patterns were analyzed with HBPLUS.[36] Contacting residues between the two monomers were determined with the program CONTACTS, using a distance cutoff of 3.66 Å. Differences in residue accessibility and solvent-exposed surfaces among the six hHexB monomers were analyzed with AREAIMOL.[31] Representations of protein topography and protein–ligand interactions were generated with TOPS[37] and LIGPLOT,[38] respectively. Molecular images were drawn with MOLSCRIPT[39] and Raster3D[40] using a graphical interface developed by N. Strater (unpublished results). Electron density representations were generated with CONSCRIPT,[41] molecular surfaces were calculated with MSMS.[42]

Protein Data Bank accession number

The atomic coordinates and structure factors have been deposited with the RCSB Protein Data Bank as entry pdb 1o7a.

Acknowledgements

We thank Claudia Alings for excellent technical assistance in protein crystallization, Judith Weissgerber and Michaela Wendeler for assistance in insect cell culture, Uwe Müller and Steffi Arzt for support at BAMline, BESSY (Berlin) and ID14 EH1, ESRF (Grenoble), respectively. These studies were supported by Deutsche Forschungsgemeinschaft (SFB 284 and Sa196/38-2), a Boehringer Ingelheim Foundation scholarship to C.S., Fonds der chemischen Industrie and Sommerfeld Stiftung.

References

1. Proia, R. L. (1988). Gene encoding the human beta-hexosaminidase beta chain: extensive homology of intron placement in the alpha- and beta-chain genes. *Proc. Natl Acad. Sci. USA*, **85**, 1883–1887.
2. Korneluk, R. G., Mahuran, D. J., Neote, K., Klavins, M. H., O'Dowd, B. F., Tropak, M. *et al.* (1986). Isolation of cDNA clones coding for the alpha-subunit of human beta-hexosaminidase. Extensive homology between the alpha- and beta-subunits and studies on Tay–Sachs disease. *J. Biol. Chem.* **261**, 8407–8413.
3. Sonderfeld-Fresko, S. & Proia, R. L. (1988). Synthesis and assembly of a catalytically active lysosomal

enzyme, beta-hexosaminidase B, in a cell-free system. *J. Biol. Chem.* **263**, 13463–13469.
4. Proia, R. L., d'Azzo, A. & Neufeld, E. F. (1984). Association of alpha- and beta-subunits during the biosynthesis of beta-hexosaminidase in cultured human fibroblasts. *J. Biol. Chem.* **259**, 3350–3354.
5. Gravel, A., Kaback, M., Proia, R. L., Sandhoff, K., Suzuki, K. & Suzuki, K. (2001). The GM2 gangliosidoses. In *The Metabolic and Molecular Bases of Inherited Diseases* (Scriver, C. R., Beaudet, A. L., Sly, W. S. & Valle, D., eds), 8th edit., **3**, pp. 3827–3877, McGraw-Hill, New York.
6. Kytzia, H. J. & Sandhoff, K. (1985). Evidence for two different active sites on human beta-hexosaminidase A. Interaction of GM2 activator protein with beta-hexosaminidase A. *J. Biol. Chem.* **260**, 7568–7572.
7. Meier, E. M., Schwarzmann, G., Furst, W. & Sandhoff, K. (1991). The human GM2 activator protein. A substrate specific cofactor of beta-hexosaminidase A. *J. Biol. Chem.* **266**, 1879–1887.
8. Hepbildikler, S. T., Sandhoff, R., Kolzer, M., Proia, R. L. & Sandhoff, K. (2002). Physiological substrates for human lysosomal beta-hexosaminidase S. *J. Biol. Chem.* **277**, 2562–2572.
9. Tews, I., Perrakis, A., Oppenheim, A., Dauter, Z., Wilson, K. S. & Vorgias, C. E. (1996). Bacterial chitobiase structure provides insight into catalytic mechanism and the basis of Tay–Sachs disease. *Nature Struct. Biol.* **3**, 638–648.
10. Schuette, C. G., Weisgerber, J. & Sandhoff, K. (2001). Complete analysis of the glycosylation and disulfide bond pattern of human beta-hexosaminidase B by MALDI-MS. *Glycobiology*, **11**, 549–556.
11. Mark, B. L., Vocadlo, D. J., Knapp, S., Triggs-Raine, B. L., Withers, S. G. & James, M. N. (2001). Crystallographic evidence for substrate-assisted catalysis in a bacterial beta-hexosaminidase. *J. Biol. Chem.* **276**, 10330–10337.
12. Prag, G., Papanikolau, Y., Tavlas, G., Vorgias, C. E., Petratos, K. & Oppenheim, A. B. (2000). Structures of chitobiase mutants complexed with the substrate Di-*N*-acetyl-D-glucosamine: the catalytic role of the conserved acidic pair, aspartate 539 and glutamate 540. *J. Mol. Biol.* **300**, 611–617.
13. Pennybacker, M., Schuette, C. G., Liessem, B., Hepbildikler, S. T., Kopetka, J. A., Ellis, M. R. *et al.* (1997). Evidence for the involvement of Glu355 in the catalytic action of human beta-hexosaminidase B. *J. Biol. Chem.* **272**, 8002–8006.
14. Jones, S. & Thornton, J. M. (1996). Principles of protein–protein interactions. *Proc. Natl Acad. Sci. USA*, **93**, 13–20.
15. Wright, C. S., Li, S. C. & Rastinejad, F. (2000). Crystal structure of human GM2-activator protein with a novel beta-cup topology. *J. Mol. Biol.* **304**, 411–422.
16. Zhang, Z. X., Wakamatsu, N., Akerman, B. R., Mules, E. H., Thomas, G. H. & Gravel, R. A. (1995). A second, large deletion in the HEXB gene in a patient with infantile Sandhoff disease. *Hum. Mol. Genet.* **4**, 777–780.
17. Prevelige, P. & Fasman, G. D. (1989). Chou–Fasman prediction of secondary structure. In *Prediction of Protein Structure and the Principles of Protein Conformation* (Fasman, G. D., ed.), pp. 1–91, Plenum, New York.
18. Wakamatsu, N., Kobayashi, H., Miyatake, T. & Tsuji, S. (1992). A novel exon mutation in the human beta-hexosaminidase beta subunit gene affects 3′ splice site selection. *J. Biol. Chem.* **267**, 2406–2413.
19. Gomez-Lira, M., Sangalli, A., Mottes, M., Perusi, C., Pignatti, P. F., Rizzuto, N. & Salviati, A. (1995). A common beta hexosaminidase gene mutation in adult Sandhoff disease patients. *Hum. Genet.* **96**, 417–422.
20. McInnes, B., Potier, M., Wakamatsu, N., Melancon, S. B., Klavins, M. H., Tsuji, S. & Mahuran, D. J. (1992). An unusual splicing mutation in the HEXB gene is associated with dramatically different phenotypes in patients from different racial backgrounds. *J. Clin. Invest.* **90**, 306–314.
21. Banerjee, P., Siciliano, L., Oliveri, D., McCabe, N. R., Boyers, M. J., Horwitz, A. L. *et al.* (1991). Molecular basis of an adult form of beta-hexosaminidase B deficiency with motor neuron disease. *Biochem. Biophys. Res. Commun.* **181**, 108–115.
22. Bolhuis, P. A., Ponne, N. J., Bikker, H., Baas, F. & Vianney de Jong, M. (1993). Molecular basis of an adult form of Sandhoff disease: substitution of glutamine for arginine at position 505 of the beta-chain of beta-hexosaminidase results in a labile enzyme. *Biochim. Biophys. Acta*, **1182**, 142–146.
23. Hou, Y., McInnes, B., Hinek, A., Karpati, G. & Mahuran, D. (1998). A Pro504 → Ser substitution in the beta-subunit of beta-hexosaminidase A inhibits alpha-subunit hydrolysis of GM2 ganglioside, resulting in chronic Sandhoff disease. *J. Biol. Chem.* **273**, 21386–21392.
24. Kuroki, Y., Itoh, K., Nadaoka, Y., Tanaka, T. & Sakuraba, H. (1995). A novel missense mutation (C522Y) is present in the beta-hexosaminidase beta-subunit gene of a Japanese patient with infantile Sandhoff disease. *Biochem. Biophys. Res. Commun.* **212**, 564–571.
25. Navon, R. & Adam, A. (1990). Thermolabile hexosaminidase (Hex) B: diverse frequencies among Jewish communities and implication for screening of sera for Hex A deficiencies. *Hum. Hered.* **40**, 99–104.
26. Narkis, G., Adam, A., Jaber, L., Pennybacker, M., Proia, R. L. & Navon, R. (1997). Molecular basis of heat labile hexosaminidase B among Jews and Arabs. *Hum. Mutat.* **10**, 424–429.
27. Yadao, F., Hechtman, P. & Kaplan, F. (1997). Formation of a ternary complex between GM2 activator protein. GM2 ganglioside and hexosaminidase A. *Biochim. Biophys. Acta*, **1340**, 45–52.
28. Liu, J., Shikhman, A. R., Lotz, M. K. & Wong, C. H. (2001). Hexosaminidase inhibitors as new drug candidates for the therapy of osteoarthritis. *Chem. Biol.* **8**, 701–711.
29. Otwinowski, Z. & Minor, W. (1997). Processing of X-ray diffraction data collected in oscillation mode. In *Macromolecular Crystallography Part A* (Carter, C. W. Jr & S, R. M., eds), **276**, pp. 307–326, Academic Press, New York.
30. Terwilliger, T. C. & Berendzen, J. (1999). Automated MAD and MIR structure solution. *Acta Crystallog. sect. D*, **55**, 849–861.
31. Collaborative Computational Project Number 4 (1994). The CCP4 suite: programs for protein crystallography. *Acta Crystallog. sect. D*, **50**, 760–763.
32. Jones, T. A. (1978). A graphics model building and refinement system for macromolecules. *J. Appl. Crystallog.* **11**, 268–272.
33. Brunger, A. T., Adams, P. D., Clore, G. M., DeLano, W. L., Gros, P., Grosse-Kunstleve, R. W. *et al.* (1998). Crystallography & NMR system: a new software suite for macromolecular structure determination. *Acta Crystallog. sect. D*, **54**, 905–921.

34. Weik, M., Ravelli, R. B., Kryger, G., McSweeney, S., Raves, M. L., Harel, M. *et al.* (2000). Specific chemical and structural damage to proteins produced by synchrotron radiation. *Proc. Natl Acad. Sci. USA*, **97**, 623–628.
35. Shindyalov, I. N. & Bourne, P. E. (1998). Protein structure alignment by incremental combinatorial extension (CE) of the optimal path. *Protein Eng.* **11**, 739–747.
36. McDonald, I. K. & Thornton, J. M. (1994). Satisfying hydrogen bonding potential in proteins. *J. Mol. Biol.* **238**, 777–793.
37. Westhead, D. R., Slidel, T. W., Flores, T. P. & Thornton, J. M. (1999). Protein structural topology: automated analysis and diagrammatic representation. *Protein Sci.* **8**, 897–904.
38. Wallace, A. C., Laskowski, R. A. & Thornton, J. M. (1995). LIGPLOT: a program to generate schematic diagrams of protein–ligand interactions. *Protein Eng.* **8**, 127–134.
39. Kraulis, P. J. (1991). MOLSCRIPT: a program to produce both detailed and schematic plots of protein structures. *J. Appl. Crystallog.* **24**, 946–950.
40. Merritt, E. A. & Bacon, D. J. (1997). Raster3D: photorealistic molecular graphics. *Methods Enzymol.* **277**, 505–524.
41. Lawrence, M. C. & Bourke, P. (2000). CONSCRIPT: a programfor generating electron density isosurfaces for presentation in protein crystallography. *J. Appl. Crystallog.* **33**, 990–991.
42. Sanner, M. F., Olson, A. J. & Spehner, J. C. (1996). Reduced surface: an efficient way to compute molecular surfaces. *Biopolymers*, **38**, 305–320.
43. Fujimaru, M., Tanaka, A., Choeh, K., Wakamatsu, N., Sakuraba, H. & Isshiki, G. (1998). Two mutations remote from an exon/intron junction in the beta-hexosaminidase beta-subunit gene affect 3′-splice site selection and cause Sandhoff disease. *Hum. Genet.* **103**, 462–469.
44. Cashman, N. R., Antel, J. P., Hancock, L. W., Dawson, G., Horwitz, A. L., Johnson, W. G. *et al.* (1986). *N*-acetyl-beta-hexosaminidase beta locus defect and juvenile motor neuron disease: a case study. *Annu. Neurol.* **19**, 568–572.

Edited by R. Huber

(Received 4 December 2002; received in revised form 20 February 2003; accepted 21 February 2003)